

Gate Fidelity and Gate Driven Dephasing via Time-Dependent Bloch-Redfield Master Equation

Sirui Chen and Dragomir Davidović

Georgia Institute of Technology, Atlanta, Georgia, United States

Understanding how the microscopic properties of open quantum systems affect gate functionality is essential for developing high-quality quantum gates. This work examines driven qubit evolution in a bath of linear harmonic oscillators with a fast external drive. The dynamically prepared state technique and the time-dependent Bloch-Redfield master equation allow for accurate state coherence calculations. This technique eliminates reaction delays for relaxation dynamics and corrects inaccurate dephasing rates caused by factorized initial states in traditional master equations. Furthermore, the interaction with the bath is investigated for its effect on gate fidelity. As a function of the qubit rotation angle, the gate fidelity is minimal for the π -flip and partially recovers with the 2π -flip.

1 Introduction

Master equations are extensively employed in quantum science to analyze dissipation and decoherence [1, 2]. There are master equations for time-independent system Hamiltonians, such as the Bloch-Redfield master equation [3], Gorini-Kossakowski-Sudarshan-Lindblad (GKSL) master equation [4, 5], as well as those for time-dependent Hamiltonians, such as Floquet master equation [6], adiabatic master equation [7, 8] and the Bloch-Redfield master equation in the interaction picture of the time-dependent Hamiltonian [9, 10]. Master equations for time-dependent Hamiltonians are particularly invaluable for investigating the interactions between qubits and external drives. Furthermore, they play a crucial role in the design and optimization of quantum control protocols.

Among various master equations, the Bloch-Redfield master equation stands out for its foundation in first-principles calculations and minimal approximations. However, the main limitation is that it leads to inaccurate populations at relaxation time-scale, with the inaccuracy of the states much higher than the inaccuracy of the generator [11, 12]. One consequence of this inaccuracy is unphysical negative eigenvalues of quantum states [13].

There indeed could be some enforced complete positivity applied, as exemplified by the GKSL master equation. The GKSL equation is usually derived using the rotating-wave approximation [14, 15] (RWA) or the secular approximation [16]. While this approach ensures complete positivity, it introduces significant errors compared to exact solutions [12, 17, 18, 19] and fails to capture non-secular dynamics.

For the Bloch-Redfield master equation, the violation of positivity occurs mostly in specific regimes where the perturbative approach is invalid [20]. Thus, the negative eigenvalues become an advantage in a sense that they signal the regime where the master equation approach is invalid. The Bloch-Redfield master equation is a potentially superior choice for studying qubit dynamics in the presence of environmental influences. By predicting the accurate coherence, it becomes a valuable tool for investigating dephasing in various quantum processes, which is of critical importance in developing scalable and high-fidelity quantum circuits [21, 22]. In this article, we explore the Bloch-Redfield equation applied to time-dependent Hamiltonians without invoking any further approximations such as the adiabatic approximation or the Floquet theory. Our study focuses on the impact of non-Markovian dynamics on relaxation, dephasing, and gate fidelity for a qubit within the spin-boson model. Moreover, we employ dynamically prepared states to achieve an even more precise characterization of the initial state of the qubit and the environment.

2 Derivation of Bloch-Redfield master equation for time-dependent Hamiltonians

To simplify our approach and enhance the readability of the text, we will begin by re-deriving the Bloch-Redfield equation in the interaction picture of a time-dependent Hamiltonian. The key derivations have been published previously [9, 10]. This discussion builds on those foundations by introducing two interaction pictures: one for pulse design and another for the system's interaction with the bath.

Consider a quantum system S that is weakly coupled to an environment B , described by the total Hamiltonian in the Schrödinger picture:

$$H = H_S(t) + H_B + H_I, \quad (1)$$

where H_B denotes the time-independent bath Hamiltonian, H_I is the time-independent interaction Hamiltonian with the bath of linear harmonic oscillators, and $H_S(t)$ represents the time-dependent qubit Hamiltonian. $H_S(t)$ can be separated into the qubit's free Hamiltonian and the control Hamiltonian $H_c(t)$

$$H_S(t) = H_0 + H_c(t) = -\frac{\Delta}{2}\sigma_z + H_c(t). \quad (2)$$

In order to analyze the evolution of the qubit, we introduce the qubit propagator

$$U_S(t) = T_{\leftarrow} e^{-i \int_0^t d\tau H_S(\tau)}. \quad (3)$$

The operator T_{\leftarrow} is the chronological time-ordering operator. Specifically the free qubit propagator $U_0 = e^{-iH_0 t}$ can be employed to express the qubit's propagator as

$$U_S(t) = U_0(t)U_c(t). \quad (4)$$

A qubit operator X in the Schrödinger picture transforms into an operator X' in the *free-propagator* interaction picture of the qubit free from both the bath and the control Hamiltonian:

$$X'(t) = U_0^\dagger(t)X(t)U_0(t). \quad (5)$$

This transformation allows for the separation of the free evolution of the system from the perturbative effects of the time-dependent perturbation $H_c(t)$, leading to the equation for the propagator

$$i \frac{dU_c}{dt} = H_c'(t)U_c \quad (6)$$

In addition, the evolution of the total density matrix in the interaction picture described by propagator $U_S(t) \otimes e^{-iH_0 t}$ of the total system is given by von Neumann equation

$$\frac{d\rho}{dt} = -i[H_I(t), \rho], \quad (7)$$

where

$$H_I(t) = U_S(t)^\dagger \otimes e^{iH_B t} H_I U_S(t) \otimes e^{-iH_B t}. \quad (8)$$

Throughout the paper, ϱ and ρ refer to a state in the interaction picture and the Schrödinger picture, respectively. Assuming an initially factorized state for the system-environment, represented as $\varrho_S(0) \otimes \varrho_B(0)$, we can expand the exponential operator into a time-ordered series. By taking the partial trace over the environmental degrees of freedom and assuming that the odd powers of the interaction Hamiltonian H_I are partially traceless, we obtain an exact expression for the reduced system's evolution:

$$\varrho_S(t) = \varrho_S(0) - \int_0^t dt_1 \int_0^{t_1} dt_2 \text{tr}_B [H_I(t_1), [H_I(t_2), [\varrho_S(0) \otimes \varrho_B(0)]]] + \dots \quad (9)$$

We assume that the initial reduced state of the environment, $\varrho_B(0)$, commutes with the bath Hamiltonian H_B , i.e., $[\varrho_B(0), H_B] = 0$. Under this assumption, ϱ_B is diagonal in the eigenbasis

of the bath Hamiltonian, which serves as the preferred basis for the bath. By taking the time derivative of Eq. 9, discarding the quadratic term, and substituting $\varrho(0)$ with $\varrho(t)$ on the right-hand side, we find the Bloch-Redfield master equation

$$\frac{d\varrho_S(t)}{dt} = -\text{Tr}_B \int_0^t ds [H_I(t), [H_I(s), \varrho_S(t) \otimes \varrho_B]]. \quad (10)$$

Furthermore, by changing the variable of integration in Eq. 10 from s to $s' = t - s$, the resulting equation would be

$$\frac{d\varrho_S(t)}{dt} = -\text{Tr}_B \int_0^t ds' [H_I(t), [H_I(t - s'), \varrho_S(t) \otimes \varrho_B]]. \quad (11)$$

This form of the time-dependent Bloch-Redfield master equation was derived previously [9, 10], and represents the straightforward extension of the Bloch-Redfield equation in the interaction picture. However, its solutions have not been widely studied yet. Assume that the interaction Hamiltonian has the following form in the Schrödinger picture:

$$H_I = \sum_{\alpha} A_{\alpha} \otimes B_{\alpha}. \quad (12)$$

where A_{α} and B_{α} are time-independent Hermitian operators acting on the system and environment, respectively. In this formulation, the physical unit is embedded in the environment's coupling operators B_{α} , leaving the system's coupling operators dimensionless.

We utilize the Fourier transform on the operator $A_{\alpha}(t) = U_S(t)^{\dagger} A_{\alpha} U_S(t)$ [10]

$$\begin{aligned} \mathcal{A}_{\alpha}(\omega) &= \int_{-\infty}^{\infty} dt A_{\alpha}(t) e^{i\omega t}, \\ A_{\alpha}(t) &= \frac{1}{2\pi} \int_{-\infty}^{\infty} d\omega \mathcal{A}_{\alpha}(\omega) e^{-i\omega t}. \end{aligned} \quad (13)$$

With this transformation, Eq. 11 is shown to be [9, 10]:

$$\frac{d\varrho_S}{dt} = \sum_{\alpha, \beta} \{ [\Lambda_{\alpha, \beta}(t) \varrho_S, A_{\alpha}(t)] + [A_{\alpha}(t), \varrho_S \Lambda_{\alpha, \beta}^{\dagger}(t)] \}, \quad (14)$$

where

$$\Lambda_{\alpha, \beta}(t) = \int_{-\infty}^{\infty} \frac{d\omega}{2\pi} \Gamma_{\alpha, \beta}(\omega, t) \mathcal{A}_{\beta}(\omega) e^{-i\omega t}. \quad (15)$$

In Eq. 15, $\Gamma_{\alpha, \beta}(\omega, t)$ represents the time-dependent spectral density, which is derived from the bath correlation function (BCF):

$$\Gamma_{\alpha, \beta}(\omega, t) = \int_0^t d\tau e^{i\omega\tau} C_{\alpha, \beta}(\tau), \quad (16)$$

where the BCF, $C_{\alpha, \beta}(\tau)$ is defined as $C_{\alpha, \beta}(\tau) = \text{Tr}_B[\rho_B B_{\alpha}(\tau) B_{\beta}(0)]$. This framework allows for the analysis of the interaction effects on the quantum system's dynamics through the spectral properties of the environment. Prior work has shown how this equation reduces to the usual Bloch-Redfield equation for time-independent Hamiltonians [10]. In the interaction picture, the latter reads the same as Eq. 14, except that the integral in Eq. 15 is substituted with the sum over discrete Bohr frequencies, e.g.,

$$\Lambda_{\alpha, \beta} = \sum_{\omega} \mathcal{A}_{\omega, \beta} e^{-i\omega t} \Gamma_{\alpha, \beta}(\omega, t), \quad (17)$$

where

$$\mathcal{A}_{\omega, \beta} = \sum_{E_m - E_n = \omega} \Pi_n A_{\alpha} \Pi_m \quad (18)$$

and Π_n are the projectors on the subspaces spanned by the eigenvectors with eigen-energy E_n .

We shall refer to the Bloch-Redfield equation for time-independent Hamiltonian as *DC-nonMarkovian*. It is non-Markovian by being sensitive to the factorized state initialization time, which is present in the spectral density in Eq. 16 through the dependence on t in the upper limit of the integral. If we take the limit $t \rightarrow \infty$ in the time-dependent spectral density in Eqs. 15 and 16, we obtain the asymptotic forms of the Bloch-Redfield equation and refer to it as *DC-Markovian*.

For a time-dependent Hamiltonian, we can also take the asymptotic limit $t \rightarrow \infty$ for the spectral density while preserving the time dependence of $A(t)$. Under this approach, Eq. 15 becomes:

$$\begin{aligned}\Lambda_{\alpha,\beta}(t) &= \int_{-\infty}^{\infty} \frac{d\omega}{2\pi} \Gamma_{\alpha,\beta}(\omega) \mathcal{A}_{\beta}(\omega) e^{-i\omega t} \\ &= \int_{-\infty}^{\infty} \frac{d\omega}{2\pi} \Gamma_{\alpha,\beta}(\omega) e^{-i\omega t} \int_{-\infty}^{\infty} A_{\beta}(\tau) e^{i\omega\tau} d\tau \\ &= \int_{-\infty}^{\infty} A_{\beta}(\tau) d\tau \int_{-\infty}^{\infty} \frac{d\omega}{2\pi} \Gamma_{\alpha,\beta}(\omega) e^{-i\omega(t-\tau)}.\end{aligned}\quad (19)$$

The second integral is $C_{\alpha,\beta}(t-\tau)\Theta(t-\tau)$ after inserting Eq. 16 where Θ is the Heaviside step function. Consequently, $\Lambda_{\alpha,\beta}(t)$ can be further simplified to

$$\Lambda_{\alpha,\beta}(t) = \int_{-\infty}^t A_{\beta}(\tau) C_{\alpha,\beta}(t-\tau) d\tau. \quad (20)$$

which reads in the Schrödinger picture as:

$$\Lambda'_{\alpha,\beta}(t) = \int_{-\infty}^t C_{\alpha,\beta}(t-\tau) U_S(t,\tau) A_{\beta} U_S(\tau,t) d\tau, \quad (21)$$

where $U_S(\tau,t) = U_S(\tau)U_S^\dagger(t)$ and $U_S(t,\tau) = U_S(\tau,t)^\dagger$.

This formulation offers a straightforward explanation for non-Markovian dynamics where the filtering operator $\Lambda'_{\alpha,\beta}(t)$ intertwines forwards and backwards time-propagations. According to Eq. 21, it propagates a state backward in time, applies the coupling operator, propagates the state forward to the present time, and finally convolves it with the bath correlation function taken between the present and passed times. As a result, the master equation depends on the history of the time-dependent perturbation. So Eq. 14 is non-Markovian, despite being time-local and independent of the initial condition.

3 Bloch-Redfield master equation for qubit in a single bath

In this work, we consider the spin-boson model with a single qubit with free Hamiltonian $H_0 = \frac{\Delta}{2}\sigma_z$ interacting with a single bath, setting $\alpha = \beta = 1$. Consequently, we will omit the bath indices in the following discussion. In the Schrödinger picture, the interaction operator for the system, denoted by A , is defined as:

$$A = \frac{1}{\sqrt{2}}(\sigma_x + \xi\sigma_z), \quad (22)$$

where ξ is the ratio between longitudinal and transverse coupling strengths. Operator A is transformed into operator $A(t)$, the coupling operator in interaction picture through the propagator defined by Eq. 4:

$$A(t) = U_S(t)^\dagger A U_S(t). \quad (23)$$

For Ohmic bath, the time-dependent spectral density $\Gamma(\omega,t) = J_\omega(t) + iS_\omega(t)$ for a single bath has the form of [10]:

$$\begin{aligned}\Gamma(\omega,t) &= -i2\lambda^2\omega_c \left\{ 1 - \frac{e^{i\omega t}}{1+i\omega_c t} - \frac{\omega}{\omega_c} e^{-\frac{\omega}{\omega_c}} \left[ei\left(\frac{\omega}{\omega_c}\right) \right. \right. \\ &\quad \left. \left. - ei\left(\frac{\omega}{\omega_c} + i\omega t\right) - i\pi\Theta\left(-\frac{\omega}{\omega_c}\right) \right] \right\}.\end{aligned}\quad (24)$$

In the limit $t \rightarrow \infty$, this expression reduces to the often used expression $J_\omega = 2\pi\lambda^2\omega\Theta(\omega)e^{-\frac{\omega}{\omega_c}}$, where λ^2 is known as the Kondo parameter. The numerical solution of Eqs. 6 and 14 was then

achieved using the Runge-Kutta 4th order method. For finite t , the integral in Eq. 15 must be computed repeatedly for each t . The computation of the asymptotic limit of the Bloch-Redfield equation ($t \rightarrow \infty$) in Eq. 15 is greatly accelerated utilizing the fast-Fourier transform. The resulting density matrix, $\rho_S(t)$, was then employed to calculate expectation values, gate-fidelity, and dephasing rates.

3.1 Liouvillian of dynamically prepared states

The generator of any trace-preserving and Hermitian-preserving semigroup can be uniquely decomposed into unitary and dissipative components [5]:

$$\frac{d\rho_S}{dt} = -i[H_{LS}(t), \rho_S] + \mathcal{D}(t)\rho_S, \quad (25)$$

where $H_{LS}(t)$ is the Lamb shift Hamiltonian, and $\mathcal{D}(t)$ represents the dissipator. The Bloch-Redfield (BR) dissipator \mathcal{D}_{BR} can be analytically derived, offering an intuitive insight into relaxation and dephasing dynamics. Starting with the tensor product basis of the Hilbert-Schmidt (HS) space in column-major order:

$$\{|0\rangle\langle 0|, |1\rangle\langle 0|, |0\rangle\langle 1|, |1\rangle\langle 1|\}, \quad (26)$$

the BR dissipator in this basis is:

$$\mathcal{D}_{BR} = \Lambda(t)^* \otimes A + A^* \otimes \Lambda(t) - \mathbb{I} \otimes A\Lambda(t) - A^*\Lambda(t)^* \otimes \mathbb{I}. \quad (27)$$

By applying a unitary transformation U , the Bloch-Redfield (BR) dissipator transforms into real matrix as $\mathcal{D}'_{BR} = U^\dagger \mathcal{D}_{BR} U$, where the unitary operator U :

$$U = \frac{1}{\sqrt{2}} \begin{bmatrix} 1 & 0 & 0 & 1 \\ 0 & 1 & i & 1 \\ 0 & 1 & -i & 0 \\ 1 & 0 & 0 & -1 \end{bmatrix}. \quad (28)$$

In this basis, the density matrix ρ is vectorized in real representation as:

$$|\rho\rangle = \frac{1}{2}[1, n_x, n_y, n_z]^\dagger, \quad (29)$$

which corresponds to the matrix:

$$\rho = \frac{1}{2}(\mathbb{I} + n_x\sigma_x + n_y\sigma_y + n_z\sigma_z). \quad (30)$$

In this representation, the first row of any generator is zero. With the coupling operator defined as in Eq. 22, the BR dissipator in the Schrödinger picture, using the form of $\Lambda(t)$ from Eq. 17, is given by:

$$\begin{bmatrix} 0 & 0 & 0 & 0 \\ -(J_\Delta - J_{-\Delta})\xi & -2J_0\xi^2 & 0 & (J_\Delta + J_{-\Delta})\xi \\ (S_\Delta + S_{-\Delta} - 2S_0)\xi & S_{-\Delta} - S_\Delta & -2J_0\xi^2 - J_\Delta - J_{-\Delta} & (S_{-\Delta} - S_\Delta)\xi \\ J_\Delta - J_{-\Delta} & 2J_0\xi & 0 & -J_\Delta - J_{-\Delta} \end{bmatrix} \quad (31)$$

where $J_\omega = \text{Re}[\Gamma(\omega, t)]$ and $S_\omega = \text{Im}[\Gamma(\omega, t)]$. The second and third rows and columns correspond to transverse (dephasing) dynamics, while the fourth row and column describes longitudinal (relaxation) dynamics. Nonsecular terms introduce mixing between these dynamics, for instance, \mathcal{D}_{42} can convert coherence into population. The spectral densities are both time and temperature dependent. In the Markovian limit at zero Kelvin, with $J_0 = J_{-\Delta} = 0$, the BR dissipator simplifies to:

$$\begin{bmatrix} 0 & 0 & 0 & 0 \\ -J_\Delta\xi & 0 & 0 & J_\Delta\xi \\ (S_\Delta + S_{-\Delta} - 2S_0)\xi & S_{-\Delta} - S_\Delta & -J_\Delta & (S_{-\Delta} - S_\Delta)\xi \\ J_\Delta & 0 & 0 & -J_\Delta \end{bmatrix} \quad (32)$$

Here, z -relaxation is decoupled from coherence dynamics, with $T_1^{-1} = \frac{J_\Delta}{2}$ representing relaxation rate. The dephasing rate, T_2^{-1} , can be obtained by diagonalizing the matrix after adding the free evolution generator:

$$\mathcal{D}'_f = \begin{bmatrix} 0 & 0 & 0 & 0 \\ 0 & 0 & \Delta & 0 \\ 0 & -\Delta & 0 & 0 \\ 0 & 0 & 0 & 0 \end{bmatrix}. \quad (33)$$

The real part of the eigenvalues reveals $T_2^{-1} = T_1^{-1}/2$, indicating no dephasing in the DC Markovian case, while the oscillation frequency is slightly modified by damping:

$$\omega_{\pm} = \pm\Delta\sqrt{1 - \frac{S_{-\Delta} - S_{\Delta}}{2\Delta(1 + \xi^2)} - \frac{J_\Delta^2}{16\Delta^2(1 + \xi^2)^2}}. \quad (34)$$

However, the BR dissipator differs when the state is dynamically prepared, as shown in Figure 1. This approach presents non-Markovian dynamics without delay in response, providing a more accurate description of relaxation and dephasing as well as the suppression of initial jolt in physical quantities. A similar approach was proposed in Ref. [23], where they applied a slow switch-on of the coupling. In contrast, our work adopts a more general method. We allow the qubit to interact with the bath and settle near its ground state before a pulse excites it into a superposition $|\psi\rangle = \frac{1}{\sqrt{2}}(|0\rangle - i|1\rangle)$. The relaxation or dephasing is then projectively measured. This method ensures minimal memory of the initial condition at the time when the pulse is delivered, allowing the non-Markovian dynamics to be caused solely by the gate.

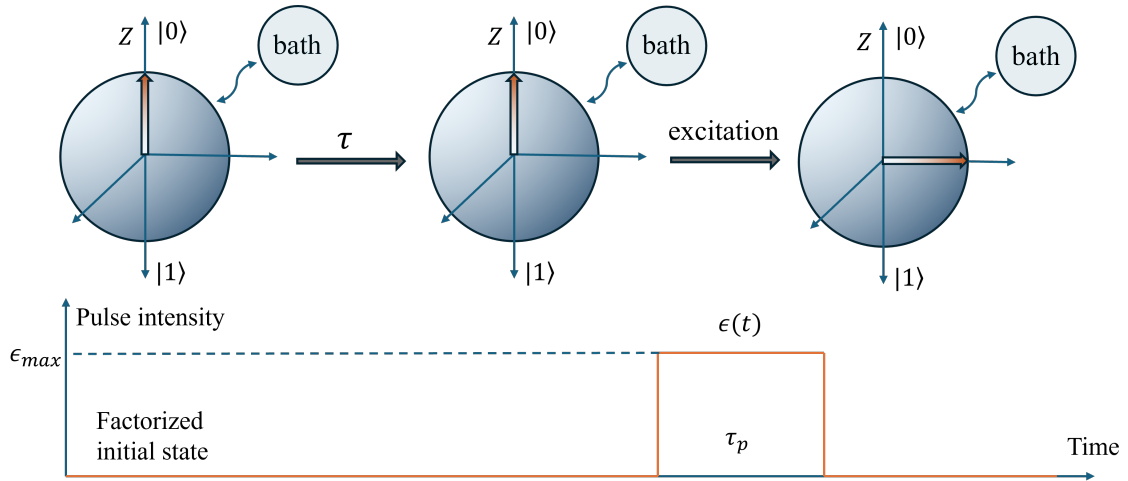


Figure 1: Schematic of the dynamically prepared state. τ represents the time allowed for system and bath to settle. In the free-propagator interaction picture, the pulse has rectangular shape with the duration τ_p .

In the free propagator interaction picture, a clean $\pi/2$ flip is represented by the operator $U_c = e^{-i\frac{\alpha}{2}\hat{n}\cdot\vec{\sigma}}$, where $\alpha = \pi/2$. For a rotation specifically in the X -direction: $U_c = e^{-i\frac{\alpha}{2}\sigma_x}$. The parameters of the control Hamiltonian are designed to make the rotation exactly $\pi/2$ in the absence of the bath. In this scenario, the dissipator can also be calculated with the help of Eqs. 20 and 21.

Let the operator $U_c(t) = e^{-i\sigma_x P(t)}$ represent the clean flip in the free-propagator interaction picture described by $e^{-iH_0 t}$, with $P(t)$ as the pulse function (see bottom of Fig. 1). Recalling Eqs. 4 and 21, the dynamically prepared $\Lambda_{dp}(\tau_m)$ in the Schrödinger picture at arbitrary measurement time τ_m after the pulse is given by:

$$\Lambda_{dp}(\tau_m) = e^{-iH_0\tau_m} U_c(\tau_m) \int_{-\infty}^{\tau_m} U_c^\dagger(\tau) e^{iH_0\tau} A e^{-iH_0\tau} U_c(\tau) C(\tau_m - \tau) d\tau U_c^\dagger(\tau_m) e^{iH_0\tau_m}. \quad (35)$$

By changing the parameter $s = \tau_m - \tau$ the expression simplifies to:

$$\Lambda_{dp}(\tau_m) = e^{-iH_0\tau_m} U_c(\tau_m) \int_0^\infty U_c^\dagger(\tau_m - s) e^{iH_0(\tau_m - s)} A e^{-iH_0(\tau_m - s)} U_c(\tau_m - s) U_c^\dagger(\tau_m) e^{iH_0\tau_m} C(s) ds. \quad (36)$$

For the DC case, where $U_c = \mathbb{I}$:

$$\Lambda_{dc}(\tau_m) = \int_0^\infty e^{-iH_0s} A e^{iH_0s} C(s) ds. \quad (37)$$

In the free propagator interaction picture the clean flip $U_c(t)$ can be expressed as:

$$U_c(t) = \mathbb{I}\Theta(\tau_{p1} - t) + U_{\frac{\pi}{2}}\Theta(t - \tau_{p2}) + e^{-i\sigma_x\epsilon(t - \tau_{p1})}\Theta(t - \tau_{p1})\Theta(\tau_{p2} - t). \quad (38)$$

τ_{p1} and τ_{p2} denotes the start and the end of the pulse. ϵ represents the amplitude of a square wave external drive. The clean flip for $\pi/2$ rotation in x direction is $U_{\frac{\pi}{2}} = e^{-i\frac{\pi}{4}\sigma_x}$ in the free propagator interaction picture. The amplitude ϵ is then $\frac{\pi}{4(\tau_{p2} - \tau_{p1})}$. Since $\tau_m > \tau_{p2}$, $U_c(\tau_m) = U_{\frac{\pi}{2}}$, then

$$U_c(\tau_m)U_c^\dagger(\tau_m - s) = U_{\frac{\pi}{2}}\Theta(\tau_{p1} - \tau_m + s) + \mathbb{I}\Theta(\tau_m - s - \tau_{p2}) + U_{\frac{\pi}{2}}e^{i\sigma_x\epsilon(\tau_m - s - \tau_{p1})}\Theta(\tau_m - s - \tau_{p1})\Theta(\tau_{p2} - \tau_m + s). \quad (39)$$

The integral for $\Lambda_{dp}(\tau_m)$ can be separated into three parts:

$$\begin{aligned} \Lambda_{dp}(\tau_m) &= \int_0^{\tau_m - \tau_{p2}} e^{-iH_0s} A e^{iH_0s} C(s) ds \\ &+ \int_{\tau_m - \tau_{p2}}^{\tau_m - \tau_{p1}} e^{-iH_0\tau_m} U_{\frac{\pi}{2}} e^{i\sigma_x\epsilon(\tau_m - s - \tau_{p1})} e^{iH_0(\tau_m - s)} A e^{-iH_0(\tau_m - s)} e^{-i\sigma_x\epsilon(\tau_m - s - \tau_{p1})} U_{\frac{\pi}{2}}^\dagger e^{iH_0\tau_m} C(s) ds \\ &+ \int_{\tau_m - \tau_{p1}}^\infty e^{-iH_0\tau_m} U_{\frac{\pi}{2}} e^{iH_0(\tau_m - s)} A e^{-iH_0(\tau_m - s)} U_{\frac{\pi}{2}}^\dagger e^{iH_0\tau_m} C(s) ds. \end{aligned} \quad (40)$$

In the first integral, $U_c(s)$ behaves identically to the DC case. In the second integral, we assume that the pulse duration is sufficiently short to make this term negligible. Without loss of generality, we set $\tau_{p1} = \tau_{p2} = \tau_d = \tau_m - u$ to represent the time of pulse arrived. Thus, the expression simplifies to:

$$\begin{aligned} \Lambda_{dp}(\tau_m) &= \int_0^u e^{-iH_0s} A e^{iH_0s} C(s) ds \\ &+ \int_u^\infty e^{-iH_0\tau_m} U_{\frac{\pi}{2}} e^{iH_0(\tau_m - s)} A e^{-iH_0(\tau_m - s)} U_{\frac{\pi}{2}}^\dagger e^{iH_0\tau_m} C(s) ds. \end{aligned} \quad (41)$$

The difference between the dynamically prepared and the DC dissipators, denoted as $\delta\Lambda(\tau_m) = \Lambda_{dp}(\tau_m) - \Lambda_{dc}(\tau_m)$, simplifies to:

$$\begin{aligned} \delta\Lambda(\tau_m) &= \int_u^\infty e^{-iH_0\tau_m} U_{\frac{\pi}{2}} e^{iH_0(\tau_m - s)} A e^{-iH_0(\tau_m - s)} U_{\frac{\pi}{2}}^\dagger e^{iH_0\tau_m} C(s) ds \\ &- \int_u^\infty e^{-iH_0s} A e^{iH_0s} C(s) ds. \end{aligned} \quad (42)$$

By defining

$$U_R(\tau_m) = e^{-iH_0\tau_m} U_{\frac{\pi}{2}} e^{iH_0\tau_m}, \quad (43)$$

the expression for $\delta\Lambda(\tau_m)$ is further simplified to:

$$\delta\Lambda(\tau_m) = U_R(\tau_m) \left[\int_u^\infty e^{-iH_0s} A e^{iH_0s} C(s) ds \right] U_R^\dagger(\tau_m) - \int_u^\infty e^{-iH_0s} A e^{iH_0s} C(s) ds. \quad (44)$$

By substituting the difference $\delta\Lambda = \Lambda_{dp}(\tau_m) - \Lambda_{dc}(\tau_m)$ into Eq. 27, and assuming that the state preparation time is sufficiently long, we retain only terms up to order τ_m^{-1} and τ_d^{-1} , discarding

faster-decaying terms, e.g., τ_m^{-2} and τ_d^{-2} . With some algebra, we then derive the difference between the DC and dynamically prepared BR dissipators, $\delta\mathcal{D}'_{BR}$, at an arbitrary measurement time τ_m after the pulse, in the regime where the time delay satisfies $u \gg \frac{1}{\omega_c}$ and $u \gg \frac{1}{\Delta}$ (for detailed discussion, see A.1).

$$\delta\mathcal{D}'_{BR} = \gamma(u) \begin{bmatrix} 0 & 0 & 0 & 0 \\ 0 & -\xi^2\omega_c & 0 & \xi^2\omega_c M \\ 0 & -G\omega_c & -\xi^2\omega_c - \xi\omega_c M & -\xi^2\omega_c G \\ 0 & \xi\omega_c & 0 & -\xi\omega_c M \end{bmatrix}, \quad (45)$$

where

$$\begin{aligned} \gamma(u) &= \frac{4\lambda^2 u \omega_c}{u^2 \omega_c^2 + 1}; \\ G &= \cos \Delta\tau_m; \\ M &= \sin \Delta\tau_m. \end{aligned} \quad (46)$$

The fast oscillating terms $G = \cos \Delta\tau_m$ and $M = \sin \Delta\tau_m$ averages out in the evolution of density matrix described by Eq. 25, at the relaxation and decoherence time-scales, leading to $G = M = 0$. Hence Eq. 45 reduce simply to:

$$\delta\mathcal{D}'_{BR} = \gamma(u) \begin{bmatrix} 0 & 0 & 0 & 0 \\ 0 & -\xi^2\omega_c & 0 & 0 \\ 0 & 0 & -\xi^2\omega_c & 0 \\ 0 & \xi\omega_c & 0 & 0 \end{bmatrix}. \quad (47)$$

The comparison of Eq. 31, Eq. 32, and Eq. 45 reveals that dynamical preparation introduces additional terms in \mathcal{D}_{22} , \mathcal{D}_{33} , and \mathcal{D}_{42} , effectively making $J_0 = \frac{\gamma\omega_c}{2}$ and the pure dephasing rate $T_\phi^{-1} = T_2^{-1} - \frac{T_1^{-1}}{2}$ non-zero. In this scenario, the coherence of the state is described by:

$$\frac{d\rho_{12}(u)}{du} = -\gamma(u)\xi^2\omega_c\rho_{12}(u), \quad (48)$$

where u denotes the time delay $\tau_m - \tau_d$. If we take the end of the pulse as the $t = 0$,

$$\frac{d\rho_{12}(t)}{dt} = -\gamma(t)\xi^2\omega_c\rho_{12}(t). \quad (49)$$

For the DC non-Markovian case, J_0 in Eq. 31 is given by the integration of the bath correlation function:

$$J_0 = \text{Re} \int_0^t C(\tau) d\tau = \frac{2\lambda^2 t \omega_c^2}{1 + t^2 \omega_c^2}. \quad (50)$$

The coherence of the state in DC non-Markovian case is then described by:

$$\frac{d\rho_{12,dc}(t)}{dt} = -2\xi^2 J_0 \rho_{12,dc}(t) = -\gamma(t)\xi^2\omega_c\rho_{12,dc}(t). \quad (51)$$

Hence the dephasing behavior of dynamically prepared states is identical with that of factorized initial state for sufficiently large u , with noticeable differences when u is modest. This indicates that dephasing can still occur at zero temperature in the dynamically prepared state, as corroborated by the numerical simulations presented in the later section. The dephasing following the pulse is non-Markovian due to the dependence of γ on the measurement time τ_m .

In comparison, the relaxation dynamics of the dynamically prepared state are equivalent to that in the DC-Markovian case, except in slow bath regimes ($\omega_c \ll \Delta$), since $\mathcal{D}'_{41} = \mathcal{D}'_{44} = 0$. The relaxation dynamics will be studied in depth next.

3.2 Relaxation of dynamically prepared states

We expect that the non-Markovian dynamics of the Bloch-Redfield equation are relevant in gates running at speeds faster than or similar to the bath correlation time $\tau_c = 1/\omega_c$. This raises the question of how fast gates impact qubit relaxation. In the DC situation (time-independent

Hamiltonian), the relaxation of the qubit from the excited state varies significantly between the non-Markovian and Markovian versions of the Bloch-Redfield equation. The factorized initial state leads to a delayed relaxation response [24], while the Markovian master equation results in a linear response at $t = 0$, with no delay in relaxation.

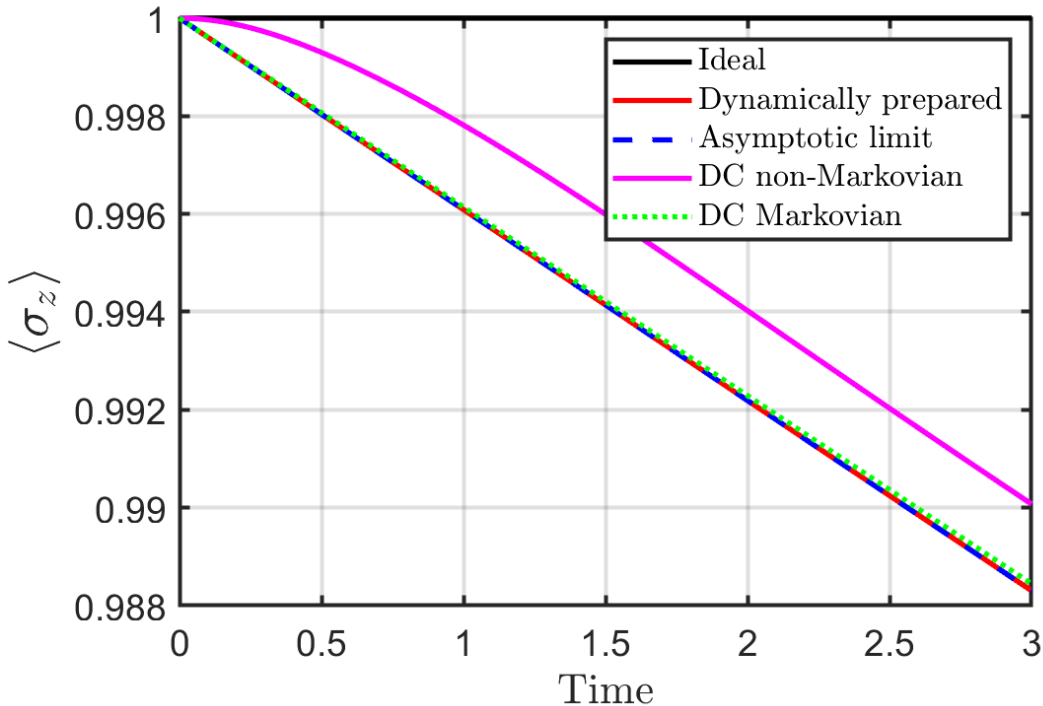


Figure 2: The relaxation of 4 different cases. Parameters chosen are $\Delta = 1$, $\lambda^2 = 0.01$, $\omega_c = 1$, $\tau_c = 1$, $\tau_p = 0.1$, $\xi = 1$, $T = 0$ and $s = 1$ (Ohmic bath).

Dynamic preparation of the initial state mitigates the discrepancy by showing that the Markovian relaxation prevails. Simulation results in Fig. 2 illustrates the time delay associated with the factorized initial state compared to the dynamically prepared state. In the DC case, there is a time delay in relaxation, referred to as the initial slip, while in the dynamically prepared case, the relaxation begins with linear time dependence and has no time delay. This graph clearly demonstrates that the slip no longer exists in the dynamically prepared state. It also indicates that the DC Markovian dynamics and non-Markovian dynamics for dynamically prepared state resemble each other, consistent with the conclusions drawn in section 3.1. Another point to note in this figure is that taking the asymptotic limit in Eq. 16 (blue dashed line) closely mirrors the behavior of the original version of Eq. 16 for the dynamically prepared state. This graph shows that the state is well prepared by the method of dynamical preparation and is insensitive to the initial condition, thus allowing this method to capture non-Markovian dynamics while not being affected by the delay in response caused by the initial condition.

3.3 Dephasing of dynamically prepared states

Dephasing refers to the loss of phase coherence between the components of a quantum superposition without any energy exchange with the environment [25]. This process is characterized by the pure dephasing rate ν_ϕ , given by the inverse of the dephasing time $\nu_\phi = \frac{1}{T_\phi}$. The relation between pure dephasing rate ν_ϕ , relaxation rate ν_1 and decoherence rate ν_2 is well known [26]:

$$\nu_2 = \frac{\nu_1}{2} + \nu_\phi. \quad (52)$$

Research suggests that using a factorized initial state, such as $\rho_S(0) \otimes \rho_B(0)$, can lead to

inaccuracies in predicting dephasing rates [26, 27]. The dephasing rate also strongly depends on whether we analyze non-Markovian dynamics or asymptotic Markovian dynamics. For example, in an Ohmic bath at zero temperature, the DC non-Markovian case can have considerable phase loss, but the DC Markovian equation has zero pure dephasing.

Introducing dynamically prepared states mitigates this discrepancy [23, 28]. We shall now show that the dephasing of dynamically prepared states is similar to the DC non-Markovian dephasing. This result differs significantly from the preceding section, in which we demonstrated very good agreement between the relaxations in the DC-Markovian master equation and that of the dynamically prepared state. This phenomenon is expected, as the flip applied to the dynamically prepared state introduces additional terms related to dephasing dynamics, but not to relaxation dynamics, in the BR dissipator, as discussed in Section 3.1.

We first allow the state to settle near ground state $|0\rangle$, then use a fast drive pulse to excite it into a superposition $|\psi\rangle = \frac{1}{\sqrt{2}}(|0\rangle - i|1\rangle)$, and subsequently observe the dephasing.

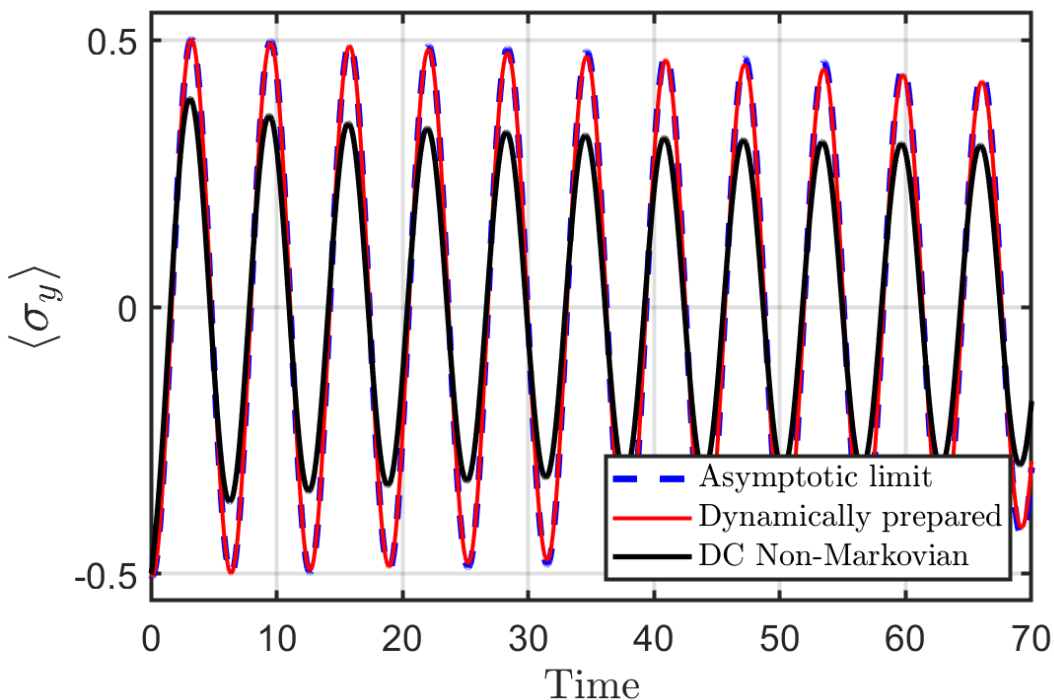


Figure 3: The oscillation of $\langle \sigma_y \rangle$ for a single qubit generated using the master equations. Here the chosen parameters are $\Delta = 1$, $\lambda^2 = 0.005$, $\omega_c = 5$, $\tau_c = 0.2$, $\tau_p = 0.1$, $\xi = 10$, $T = 0$ and $s = 1$.

Fig. 3 shows the simulation results of the time-dependent Redfield master equation, comparing the dephasing behaviors for factorized initial states and dynamically prepared state. In the DC non-Markovian case, the factorized initial state (black, solid line) exhibits a sudden jolt at the beginning, while the DC Markovian case has no pure dephasing at all [26]. This unphysical jolt in physical quantities, also reported in previous studies [23], is attributed to an imbalanced initial condition. Such discrepancies highlight the limitations of using factorized initial conditions in accurately modeling system-environment interactions in quantum systems. In contrast, the dynamically prepared state (red solid and blue dashed line) shows a more gradual dephasing. The dephasing behaviour is similar with the DC non-Markovian case after the initial discrepancy. Thus the dephasing induced by the gate is non-Markovian, consistent with the analytical predictions presented in Section 3.1, as demonstrated in Eq. 48.

Through Eq. 52 we can determine the decoherence rate ν_2 and the relaxation rate ν_1 through fitting, and subsequently calculate the pure dephasing rate ν_ϕ under various conditions. This method allows for precise exploration of the dependence of ν_ϕ on different gate parameters.

Fig. 4 presents the simulation results illustrating the dependence of the pure dephasing rate ν_ϕ

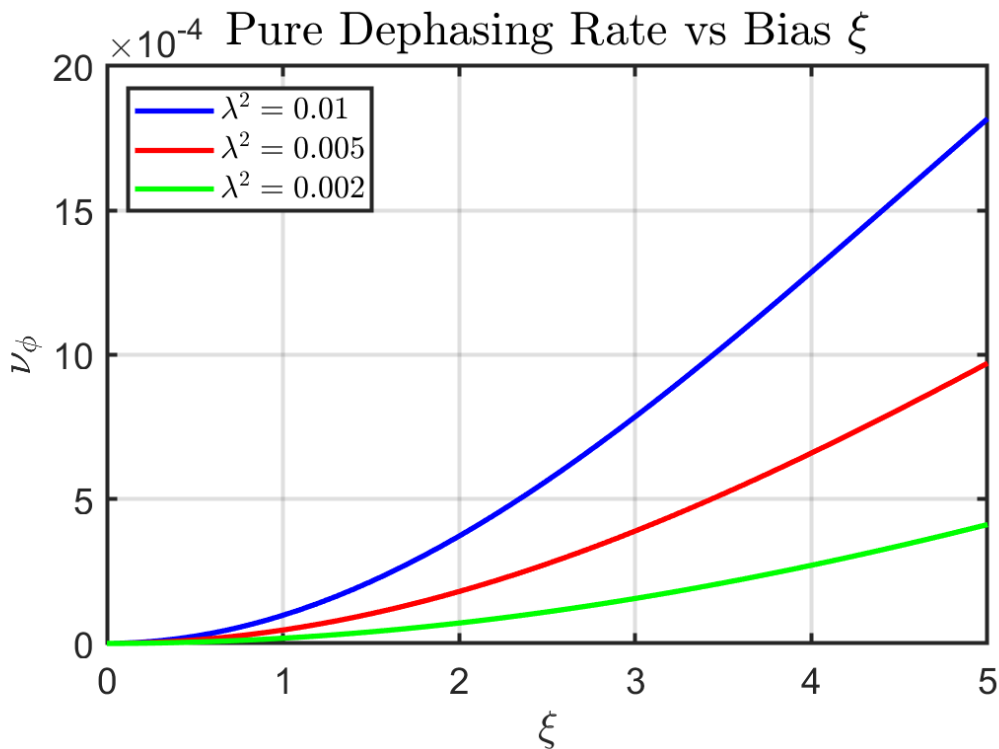


Figure 4: The pure dephasing rate ν_ϕ of dynamically prepared state as a function of the bias ξ in the coupling operator. The parameters for the bath are $\omega_c = 5$, $\tau_c = 0.2$, $T = 0$ and $s = 1$. The time duration of pulse is $\tau_p = 0.1$.

on the bath bias ξ obtained by solving the dynamically prepared Bloch-Redfield master equation. In Eq. 22, ξ is associated with the σ_z component of the coupling operator. As ξ approaches 0, the pure dephasing rate ν_ϕ saturates at 0, independent of λ^2 within the weak coupling regime, thus, the dephasing of the dynamically prepared state approaches the DC Markovian case at zero bias. This result is consistent with the previous analytical derivation. In Eq. 47, we show that when $\xi = 0$, the difference in Liouvillian $\delta\mathcal{D}'_{BR}$ is 0, thus giving the same zero dephasing as the DC Markovian case.

The temperature T affects the spectral density function of the bath, thereby influencing the pure dephasing rate. Fig. 5 depicts the temperature dependence of the dephasing rates in dynamically prepared states. As the temperature approaches zero, the dephasing rate saturates. But the rates still maintain their high temperature scaling. In the low temperature limit $T \rightarrow 0$, the residual dephasing rate is determined by the effective $J_0 = \frac{\gamma\omega_c}{2}$.

As demonstrated in the two examples, the Bloch-Redfield master equation, known for its precision in calculating coherence [10, 23], when combined with dynamically prepared states that address the limitations of factorized initial states, provides a promising and efficient tool for studying dephasing dynamics in quantum computing. This approach enhances the accuracy of coherence calculations and offers a realistic depiction of non-Markovian dynamics.

3.4 Gate fidelity

Another application of the time-dependent Bloch-Redfield quantum master equation in conjunction with dynamically prepared states is in fidelity examination. In real quantum circuits, numerous factors can influence operational fidelity [29], such as pulse strength, pulse shape [30], and specific control sequences [31, 32]. The time-dependent Bloch-Redfield master equation allows for the simulation of quantum operations starting from the microscopic Hamiltonian of the system. This approach opens the possibility to study how microscopic parameters affect driving pulse protocols. In this paper, we provide an example of optimizing fidelity by adjusting pulse length, though the

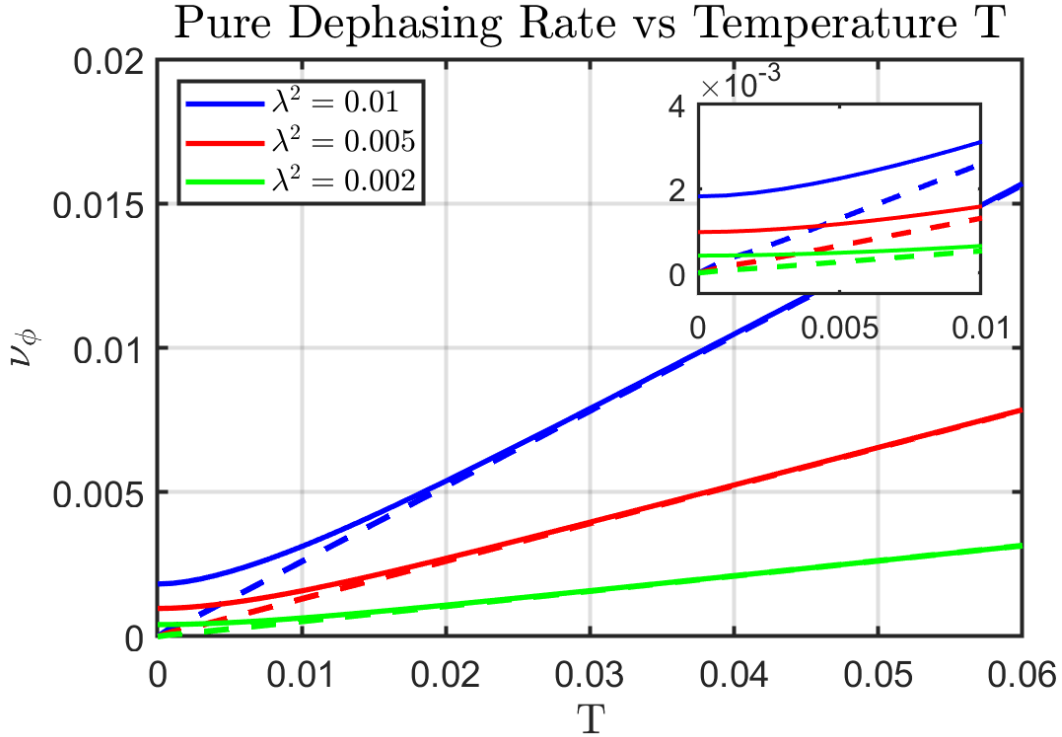


Figure 5: The pure dephasing rate ν_ϕ of dynamically prepared state is plotted as a function of temperature T . The bath parameters are set to $\omega_c = 5$, $\tau_c = 0.2$, $\xi = 5$ and $s = 1$. The time duration of pulse is $\tau_p = 0.1$. Dashed lines are the dephasing rate calculated in the DC Markovian case.

full potential of our method remains to be explored.

As we introduced in Sec. 3.1 the clean flip rotation is determined by the pulse intensity ϵ . Here we use the fidelity defined according to the trace distance between the density matrix $\rho(\epsilon)$ simulated by the dynamically prepared Bloch-Redfield equation and the pure state $\rho'(\theta, \phi)$. θ and ϕ denotes the polar angle and azimuthal angle of a Bloch vector $\vec{r} = (r \sin \theta \cos \phi, r \sin \theta \sin \phi, r \cos \theta)$ on the Bloch sphere (for mixed states $r < 1$). Density matrix for pure state is then $\rho(\theta, \phi) = \frac{1}{2}(\mathbb{I} + \vec{r} \cdot \vec{\sigma})$. The trace distance is calculated through Singular Value Decomposition (SVD):

$$\rho(\epsilon) - \rho'(\theta, \phi) = U \Sigma V^\dagger. \quad (53)$$

Here, U and V are unitary matrices, and Σ is a diagonal matrix with nonnegative diagonal elements $\{\sigma_i\}$. The trace distance is then $D = \frac{1}{2} \sum_i \sigma_i$. The fidelity F of the flip is defined as:

$$F(\epsilon, \theta, \phi) = 1 - \frac{1}{2} \sum_i \sigma_i. \quad (54)$$

The pulse amplitude ϵ is set to achieve the desired flip angle, such as $\pi/2$ or $3\pi/2$, in the absence of a bath. For a perfect $\pi/2$ rotation about the X axis, the target state is $\rho_t(\theta = \pi/2, \phi = -\pi/2)$, and the maximum fidelity should ideally occur at $F(\epsilon, \theta = \pi/2, \phi = -\pi/2)$. However, due to bath-induced effects during the gate operation, the resulting state is neither pure nor precisely located at $\theta = \pi/2, \phi = -\pi/2$. The shift in the location of the fidelity maximum within the θ, ϕ parameter space serves as an indicator of the latency and phase noise induced by the gate's interaction with the bath.

In this study, we measure the gate fidelity at time τ_m , following the end of the pulse. To completely account for the effect of the entire pulse, τ_m should be significantly larger than $\tau_c = 1/\omega_c$, which is the bath correlation time. To distinguish between the intrinsic contribution of the gate and free relaxation and dephasing, τ_m is significantly smaller than the relaxation and dephasing times. In this work, we set $\tau_m = 25\tau_c$ little less than one cycle of the qubit, without losing generality.

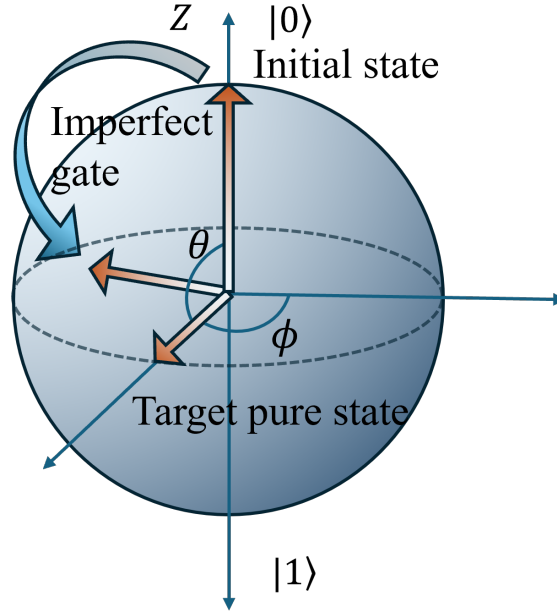


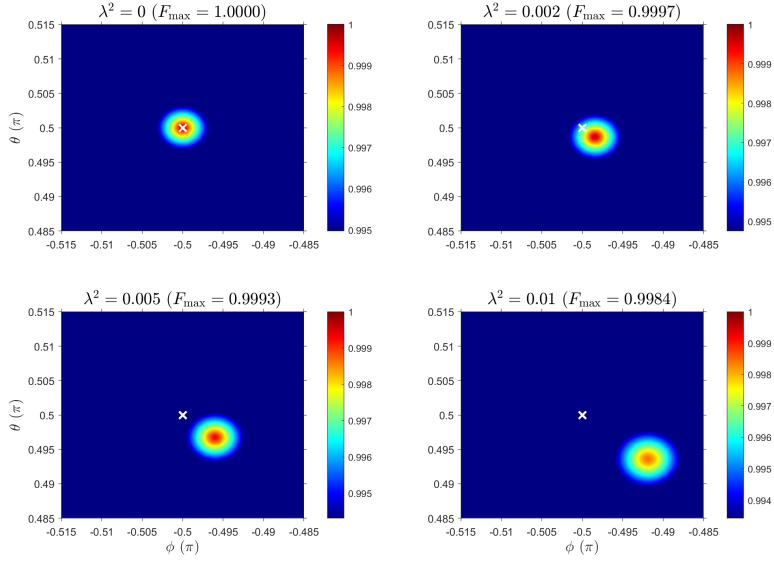
Figure 6: Schematic graph of an imperfect gate. The interaction with the bath causes a deviation from the desired pure state angle and a broadening of the angle distribution.

From Fig. 7a, we observe that for a $\pi/2$ pulse, which excites a qubit from the ground state to a superposition state, the maximum fidelity decreases as λ^2 increases. Additionally, the θ_m , where the fidelity is maximized, is slightly lower than the standard $\pi/2$, indicating the tendency to revert to the ground state. A slight overdrive can compensate for this tendency and bring the angle of peak fidelity at $\pi/2$. Moreover, the ϕ_m also deviates from the ideal case, which can also be corrected by pulse design. However, even with optimal θ and ϕ adjustment, the maximum fidelity still falls short of unity.

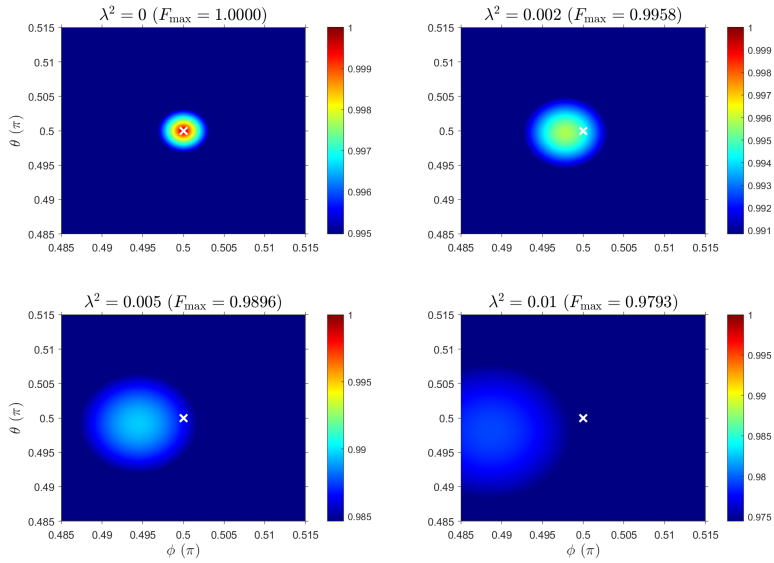
The shifts in θ_m and ϕ_m are due to anisotropic spread out of the state caused by interactions with the bath. While dynamical techniques such as pulse shaping can mitigate this kind of drift, they cannot fully eliminate gate errors. Because the state's isotropic and incoherent spread out during gate operations leads to a loss of purity in the density matrix, this fundamentally limits the achievable gate fidelity.

Figure. 7b shows a reversal of drift when the target angle is $3\pi/2$, which implies the possibility of refocusing. The error induced by drift can indeed be restored through dynamical method to some extent, as shown in Fig. 8. The figure depicts the fidelity with respect to the flip angle α . The minimum gate fidelity is observed at $\alpha = \pi$. Above this angle, the fidelity increases versus α , which might be viewed as refocusing, especially when the bath bias ξ is modest. The 2π rotation mimics the spin echo, which has a continuous sequence of $\pi/2$, π , and $\pi/2$. Thus, imperfect gates can nevertheless be helpful for dynamic decoupling techniques like spin echo and CPMG sequences [31, 32].

The T_1 process in qubits is directly associated with the loss of purity. Although traditionally challenging to mitigate T_1 effects through dynamical decoupling and quantum coherent control, recent advances in Quantum Error Correction (QEC), as demonstrated in [33], have shown the potential to achieve gate fidelities beyond the T_1 limit in superconducting circuits. Thus, to further improve the gate fidelity, techniques such as dynamical decoupling gates or geometric operations could be beneficial [34, 35, 36]. These techniques can also be examined using the method described in this paper, providing an approach to optimizing qubit fidelity.



(a) The fidelity $F(\theta, \phi)$ of an $\alpha = \pi/2$ gate. We observe a drift in the parameters θ_m and ϕ_m associated with the maximum fidelity. Only values of $F(\theta, \phi)$ in the range $[0.998F_{\max}, F_{\max}]$ are plotted to represent the distribution of the state. The white cross represents the targeted state.



(b) The fidelity $F(\theta, \phi)$ of an $\alpha = 3\pi/2$ gate. Only values of $F(\theta, \phi)$ in the range $[0.998F_{\max}, F_{\max}]$ are plotted to represent the distribution of the state. The white cross represents the targeted state. The direction of the drift is reversed.

Figure 7: The fidelity of a $\pi/2$ and $3\pi/2$ gate as a function of θ and ϕ . $\lambda^2 = 0$ denotes the case of flip without the bath. The parameters for the bath are $\omega_c = 5$, $\tau_c = 0.2$, $\xi = 1$, and $s = 1$. The time duration of pulse is $\tau_p = 5.1$.

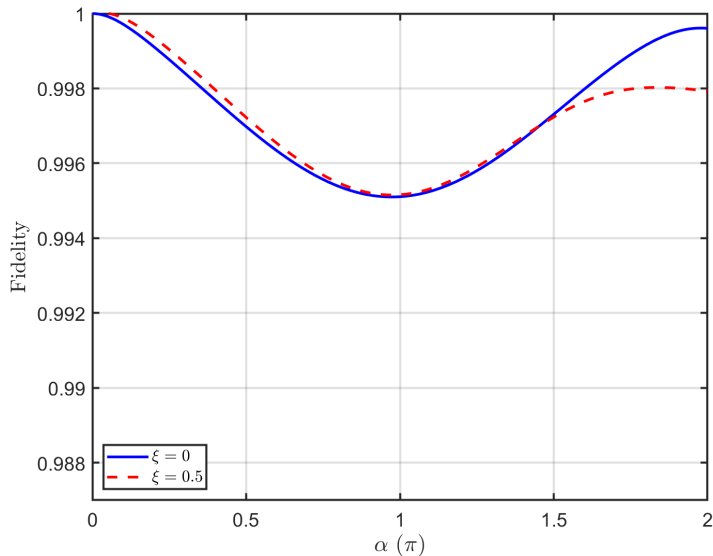


Figure 8: The fidelity versus the flip angle α . The bath parameters are set to $\lambda^2 = 0.002$, $\omega_c = 5$, $\tau_c = 0.2$ and $s = 1$. The time duration of pulse is $\tau_p = 5.1$

4 Conclusions and discussion

In this work, we utilized the time-dependent Bloch-Redfield master equation to explore driven qubit dephasing and gate fidelity under various conditions. We discussed the time-dependent Bloch-Redfield master equation for its foundation in first principles and its ability to accurately predict coherence. We have resolved the issue of initial state preparation by presenting the method of dynamical state preparation, both analytically and numerically and found very good agreement. This method allows us to precisely capture the fundamental properties of non-Markovian dynamics. The introduction of dynamically prepared states in relaxation eliminates the initial slip, suggesting that the relaxation behavior closely aligns with asymptotic Markovian behavior. The dephasing process, however, markedly differs from both the asymptotic Markovian limit and the non-Markovian limit seen in the case of a factorized initial state. The relationship between the dephasing rate and characteristics such as bias ξ and temperature T is examined, illustrating the method's capacity to precisely determine dephasing rates in driven open quantum systems. This analysis demonstrates how the approach stands between the DC Markovian and non-Markovian limits, effectively capturing non-Markovian dynamics while remaining unaffected by time delays induced by the initial condition. The behavior of relaxation dynamics and dephasing dynamics agrees well with the analytic prediction.

Building on the enhanced accuracy of our method, we further investigated gate fidelity using the time-dependent Bloch-Redfield master equation. Our findings indicate that the loss of purity induced by gate operations fundamentally limits the maximum achievable gate fidelity. Moreover, we observed that fidelity can be moderately refocused, demonstrating the reversibility of drift-induced errors and suggesting that imperfect gates can effectively support dynamical decoupling.

Future investigations building upon this work will focus on the slow bath regime, where $\omega_c \ll 1$. In this regime, the approximations made in Appendix A.1 become invalid, leading to dephasing and relaxation dynamics that deviate from both the DC Markovian and DC non-Markovian cases. Additionally, the sub-Ohmic regime ($s < 1$) and spin-baths present another area of interest, as $1/f$ noise, which is prevalent in the sub-Ohmic regime, is known to induce significant dephasing in practical quantum circuits. By utilizing the dynamically prepared Redfield master equation, it is possible to explore the dynamics associated with the spin-baths [37] and $1/f$ noise and potentially identify strategies for mitigating its effects such as dynamical decoupling.

We thank Jiahao Chen, Elyana Crowder, Nicholas Ezzell and Daniel Lidar for fruitful discussions. Support by the school of physics in Georgia Institute of technology is gratefully acknowl-

edged.

References

- [1] M. S. Sarandy and D. A. Lidar. Adiabatic quantum computation in open systems. *Phys. Rev. Lett.*, 95:250503, Dec 2005.
- [2] Frank Verstraete, Michael M Wolf, and J Ignacio Cirac. Quantum computation and quantum-state engineering driven by dissipation. *Nature physics*, 5(9):633–636, 2009.
- [3] Alfred G Redfield. On the theory of relaxation processes. *IBM Journal of Research and Development*, 1(1):19–31, 1957.
- [4] G. Lindblad. On the generators of quantum dynamical semigroups. *Communications in Mathematical Physics*, 48(2):119–130, June 1976.
- [5] Vittorio Gorini, Andrzej Kossakowski, and Ennackal Chandu George Sudarshan. Completely positive dynamical semigroups of n-level systems. *Journal of Mathematical Physics*, 17(5):821–825, 1976.
- [6] Jon H. Shirley. Solution of the schrödinger equation with a hamiltonian periodic in time. *Phys. Rev.*, 138:B979–B987, May 1965.
- [7] Herbert Spohn. Kinetic equations from hamiltonian dynamics: Markovian limits. *Reviews of Modern Physics*, 52(3):569, 1980.
- [8] Tameem Albash, Sergio Boixo, Daniel A Lidar, and Paolo Zanardi. Quantum adiabatic markovian master equations. *New Journal of Physics*, 14(12):123016, 2012.
- [9] Huo Chen and Daniel A Lidar. Hamiltonian open quantum system toolkit. *Communications Physics*, 5(1):112, 2022.
- [10] Dragomir Davidović. Geometric-arithmetic master equation in large and fast open quantum systems. *Journal of Physics A: Mathematical and Theoretical*, 55(45):455301, 2022.
- [11] C. H. Fleming and N. I. Cummings. Accuracy of perturbative master equations. *Phys. Rev. E*, 83:031117, Mar 2011.
- [12] Devashish Tupkary, Abhishek Dhar, Manas Kulkarni, and Archak Purkayastha. Fundamental limitations in lindblad descriptions of systems weakly coupled to baths. *Physical Review A*, 105(3):032208, 2022.
- [13] Robert S Whitney. Staying positive: going beyond lindblad with perturbative master equations. *Journal of Physics A: Mathematical and Theoretical*, 41(17):175304, 2008.
- [14] Edwin T Jaynes and Frederick W Cummings. Comparison of quantum and semiclassical radiation theories with application to the beam maser. *Proceedings of the IEEE*, 51(1):89–109, 1963.
- [15] Bruce W Shore and Peter L Knight. The jaynes-cummings model. *Journal of Modern Optics*, 40(7):1195–1238, 1993.
- [16] E Brian Davies. Markovian master equations. *Communications in mathematical Physics*, 39:91–110, 1974.
- [17] Amro Dodin, Timur Tscherbul, Robert Alicki, Amar Vutha, and Paul Brumer. Secular versus nonsecular redfield dynamics and fano coherences in incoherent excitation: An experimental proposal. *Physical Review A*, 97(1):013421, 2018.
- [18] PR Eastham, P Kirton, HM Cammack, BW Lovett, and J Keeling. Bath-induced coherence and the secular approximation. *Physical Review A*, 94(1):012110, 2016.
- [19] Elyana Crowder, Lance Lampert, Grihith Manchanda, Brian Shoffeitt, Srikar Gadamsetty, Yiting Pei, Shantanu Chaudhary, and Dragomir Davidović. Invalidation of the bloch-redfield equation in the sub-ohmic regime via a practical time-convolutionless fourth-order master equation. *Phys. Rev. A*, 109:052205, May 2024.

- [20] Richard Hartmann and Walter T Strunz. Accuracy assessment of perturbative master equations: Embracing nonpositivity. *Physical Review A*, 101(1):012103, 2020.
- [21] P. Bertet, I. Chiorescu, G. Burkard, K. Semba, C. J. P. M. Harmans, D. P. DiVincenzo, and J. E. Mooij. Dephasing of a superconducting qubit induced by photon noise. *Phys. Rev. Lett.*, 95:257002, Dec 2005.
- [22] David Kielpinski, Chris Monroe, and David J Wineland. Architecture for a large-scale ion-trap quantum computer. *Nature*, 417(6890):709–711, 2002.
- [23] CH Fleming, Albert Roura, and BL Hu. Initial-state preparation with dynamically generated system-environment correlations. *Physical Review E—Statistical, Nonlinear, and Soft Matter Physics*, 84(2):021106, 2011.
- [24] Pierre Gaspard and Masataka Nagaoka. Slippage of initial conditions for the redfield master equation. *The Journal of chemical physics*, 111(13):5668–5675, 1999.
- [25] Anthony J Leggett, SDAFMGA Chakravarty, Alan T Dorsey, Matthew PA Fisher, Anupam Garg, and Wilhelm Zwerger. Dynamics of the dissipative two-state system. *Reviews of Modern Physics*, 59(1):1, 1987.
- [26] Angel Rivas and Susana F Huelga. *Open quantum systems*, volume 10. Springer, 2012.
- [27] Heinz-Peter Breuer, Elsi-Mari Laine, Jyrki Piilo, and Bassano Vacchini. Colloquium: Non-markovian dynamics in open quantum systems. *Reviews of Modern Physics*, 88(2):021002, 2016.
- [28] Jonas Richter, Mats H. Lamann, Christian Bartsch, Robin Steinigeweg, and Jochen Gemmer. Relaxation of dynamically prepared out-of-equilibrium initial states within and beyond linear response theory. *Phys. Rev. E*, 100:032124, Sep 2019.
- [29] Philip Krantz, Morten Kjaergaard, Fei Yan, Terry P Orlando, Simon Gustavsson, and William D Oliver. A quantum engineer’s guide to superconducting qubits. *Applied physics reviews*, 6(2), 2019.
- [30] Hsiang S Ku, JL Long, Xian Wu, Mustafa Bal, RE Lake, Edwin Barnes, Sophia E Economou, and David P Pappas. Single qubit operations using microwave hyperbolic secant pulses. *Physical Review A*, 96(4):042339, 2017.
- [31] Herman Y Carr and Edward M Purcell. Effects of diffusion on free precession in nuclear magnetic resonance experiments. *Physical review*, 94(3):630, 1954.
- [32] Saul Meiboom and David Gill. Modified spin-echo method for measuring nuclear relaxation times. *Review of scientific instruments*, 29(8):688–691, 1958.
- [33] Aleksander Kubica, Arbel Haim, Yotam Vaknin, Harry Levine, Fernando Brandão, and Alex Retzker. Erasure qubits: Overcoming the t 1 limit in superconducting circuits. *Physical Review X*, 13(4):041022, 2023.
- [34] Guofu Xu and Guilu Long. Protecting geometric gates by dynamical decoupling. *Phys. Rev. A*, 90:022323, Aug 2014.
- [35] Abdufarrukh A Abdumalikov Jr, Johannes M Fink, Kristinn Juliusson, Marek Pechal, Simon Berger, Andreas Wallraff, and Stefan Filipp. Experimental realization of non-abelian non-adiabatic geometric gates. *Nature*, 496(7446):482–485, 2013.
- [36] Tongxing Yan, Bao-Jie Liu, Kai Xu, Chao Song, Song Liu, Zhensheng Zhang, Hui Deng, Zhiguang Yan, Hao Rong, Keqiang Huang, et al. Experimental realization of nonadiabatic shortcut to non-abelian geometric gates. *Physical review letters*, 122(8):080501, 2019.
- [37] Clemens Müller, Jürgen Lisenfeld, Alexander Shnirman, and Stefano Poletto. Interacting two-level defects as sources of fluctuating high-frequency noise in superconducting circuits. *Physical Review B*, 92(3):035442, 2015.

A Appendix

A.1 Analytical derivation of $\delta D'_{BR}$

For ohmic bath ($s = 1$), the bath correlation function at zero temperature is

$$C(t) = \frac{1}{\pi} \int_{-\infty}^{\infty} J_{\omega} e^{-i\omega t} d\omega = \frac{2\lambda^2 \omega_c^2}{(1 + i\omega c t)^2}. \quad (55)$$

Combining the bath correlation function with Eq. 44, the $\delta\Lambda(\tau_m)$ is then:

$$\delta\Lambda(\tau_m) = \begin{pmatrix} \frac{\sqrt{2}\lambda^2(\xi\omega_c + \frac{W}{2})}{-i + u\omega_c} & \frac{i\sqrt{2}e^{i\tau_m}\Delta\lambda^2(\xi\omega_c - \frac{W}{2})}{-i + u\omega_c} \\ \frac{i\sqrt{2}e^{-i\tau_m}\Delta\lambda^2(-\xi\omega_c + \frac{W}{2})}{-i + u\omega_c} & \frac{\sqrt{2}\lambda^2(-\xi\omega_c - \frac{W}{2})}{-i + u\omega_c} \end{pmatrix}, \quad (56)$$

where

$$\begin{aligned} W &= 2\Delta\text{Ci}(Z_u) \cos(Z_{\tau_m}) - \Delta(\pi - 2\text{Si}(Z_u)) \sin(Z_{\tau_m}) + 2\omega_c \sin(\Delta(\tau_m - u)); \\ Z_u &= \Delta\left(u - \frac{i}{\omega c}\right); Z_{\tau_m} = \Delta\left(\tau_m - \frac{i}{\omega c}\right). \end{aligned} \quad (57)$$

Ci(Z) and Si(Z) are sin-integral and cos-integral separately. Assuming that the state preparation time is sufficiently long, and the measurement delay $u \gg \frac{1}{\omega c}$, then we only consider terms up to order u^{-1} and τ_m^{-1} while discarding faster-decaying terms. The asymptotic expansions of Ci(Z) and Si(Z) at infinity are:

$$\begin{aligned} \text{Si}(Z) &= \frac{\pi}{2} + \cos Z \left(\frac{2}{Z^3} - \frac{1}{Z}\right) - \frac{\sin Z}{Z^2} + \dots \\ \text{Ci}(Z) &= \sin Z \left(-\frac{2}{Z^3} + \frac{1}{Z}\right) - \frac{\cos Z}{Z^2} + \dots \end{aligned} \quad (58)$$

In the case where τ_m and u are large enough compared to Δ^{-1} , Z is dominated by the real part and is large enough to discarding terms decaying faster than Z^{-1} . Eq. 57 then simplifies to:

$$W = 2\omega_c \sin(\Delta(\tau_m - u)) - 2\omega_c \sin(\Delta(\tau_m - u)) = 0. \quad (59)$$

We can then utilize Eq. 56 to find the difference between the dissipator of the dynamically prepared state and that of the DC case:

$$\delta\mathcal{D}_{BR} = \delta\Lambda(t)^* \otimes A + A^* \otimes \delta\Lambda(t) - \mathbb{I} \otimes A\delta\Lambda(t) - A\delta\Lambda(t)^* \otimes \mathbb{I}. \quad (60)$$

After performing the basis transformation $\delta\mathcal{D}'_{BR} = U^\dagger \delta\mathcal{D}_{BR} U$, and discarding terms decaying faster than τ_d^{-1} , we arrive at the expression 45:

$$\delta\mathcal{D}'_{BR} = \gamma(u) \begin{bmatrix} 0 & 0 & 0 & 0 \\ 0 & -\xi^2\omega_c & 0 & \xi^2\omega_c M \\ 0 & -G\omega_c & -\xi^2\omega_c - \xi\omega_c M & -\xi^2\omega_c G \\ 0 & \xi\omega_c & 0 & -\xi\omega_c M \end{bmatrix}, \quad (61)$$

where

$$\begin{aligned} \gamma(u) &= \frac{4\lambda^2 u \omega_c}{u^2 \omega_c^2 + 1}; \\ G &= \cos \Delta\tau_m; \\ M &= \sin \Delta\tau_m. \end{aligned} \quad (62)$$